# AIAA 2001-3870
# Higher Mean-Flow Approximation for a Solid Rocket Motor with Radially Regressing Walls

J. Majdalani and A. B. Vyas
Marquette University
Milwaukee, WI 53233

# 37th AIAA/ASME/SAE/ASEE Joint Propulsion Conference and Exhibit
## 8–11 July 2001, Salt Lake City, UT

# Higher Mean-Flow Approximation for a Solid Rocket Motor with Radially Regressing Walls

Joseph Majdalani* and Anand B. Vyas†
*Marquette University, Milwaukee, WI 53233*
and
Gary A. Flandro‡
*University of Tennessee Space Institute, Tullahoma, TN 37388*

In this paper, the bulk gas dynamics of an internal burning rocket motor are described using a rotational, incompressible, and viscous flow model that incorporates the effects of radial wall regression. The mathematical model developed herein is also applicable to semi-open porous tubes with expanding walls. A spatial transformation is used that takes advantage of the linear variation in the mean axial velocity. A self-similar transformation in time is also used. By applying these similarity transformations in both space and time, the Navier-Stokes equations are reduced to a single, nonlinear, fourth-order differential equation. After providing the details leading to the exact Navier-Stokes formulation, the resulting equation is solved using variation of parameters and small-parameter perturbations based on small viscosity. The asymptotic solutions for the velocity, pressure, and shear are obtained as function of the crossflow Reynolds number $R$ and the dimensionless regression ratio $\alpha$. By way of verification, we show that as $\alpha/R \to 0$ Yuan and Finkelstein's solutions can be restored from ours. Similarly, as $\alpha/R \to 0$, Taylor's or Culick's inviscid profiles are recovered. This work demonstrates that, for a range of small $\alpha/R$, inviscid solutions are practical. However, for fast burning propellants such as those being developed for high-acceleration interceptor vehicles, the inviscid assumption deteriorates. Being applicable over a wider range of physical parameters, the current analysis leads to an improved mean flow solution that may be used, instead of the inviscid model, to a) reevaluate viscous and rotational vortico-acoustic fields, b) investigate the onset of hydrodynamic instability, and c) simulate the internal flow in rapidly regressing motors.

## Nomenclature

$a$ = instantaneous wall radius, m
$\dot{a}$ = wall regression rate, m/s
$F$ = similarity function
$\overline{p}$ = dimensional pressure, Pa
$\overline{r}$ = radius, m
$r$ = normalized radial coordinate, $\overline{r}/a$
$R$ = injection Reynolds number
$t$ = time, s
$\overline{u}$ = velocity ($\overline{u}_r$, $\overline{u}_z$), m/s

$\overline{z}$ = axial coordinate, m
$z$ = normalized axial coordinate, $\overline{z}/a$
$\alpha$ = dimensionless regression ratio
$\Delta$ = difference
$\varepsilon$ = reciprocal of the injection Reynolds number
$\eta$ = transformed radial coordinate, $\frac{1}{2}r^2$
$\Omega$ = vorticity, rad/s
$\rho$ = density, kg/m$^3$
$\tau$ = normalized shear stress
$\nu$ = kinematic viscosity, m$^2$/s
$\theta$ = normalized transformation coordinate
$\psi$ = normalized stream function

*Subscripts*
m = mean value at a given cross section
r = radial component or partial derivative
s = solid phase
t = temporal derivative
b = porous boundary or burning surface
z = axial component or partial derivative

*Assistant Professor, Department of Mechanical and Industrial Engineering. Member AIAA.

†Graduate Student and Research Associate. Member AIAA.

‡Boling Chair Professor of Mechanical and Aerospace Engineering. Associate Fellow, AIAA.

# I.   Introduction

SEVERAL mathematical problems of real concern involve the motion of an injection-driven fluid inside a tube with transpiring walls.  Past and recent interests have ranged over a wide spectrum of technical applications.  These include, but are not limited to, paper making,[1] sweat cooling and heating,[2,3] flow filtration and isotope separation,[4-6] thermal and viscous boundary layer control,[7-9] and internal flow modeling in solid rocket motors.  Internal flow modeling has received considerable attention over the past four decades due to the central role that it plays in the overall assessment of rocket combustion instability.  This is due, in part, to the strong dependence of the volumetric stability integrals in solid rocket motors on the precise determination of the velocity and pressure fields.  The need to accurately describe the bulk gas motion inside rocket motors has therefore motivated, over the past years, a number of capable investigators to seek mathematical models of increasing levels of refinement.

To better understand the evolution of the problem at hand, it should first be recognized that the internal flow has been traditionally viewed as consisting of a superposition of mean and oscillatory fields.  It should also be recognized that the oscillatory field is driven, in part, by the mean flow motion.  As such, it would be certainly desirable to obtain both components under the same fundamental flow conditions and comparable levels of precision.

The first adequate mean flow solution was presented by Culick[10] and constituted a worthy improvement over the one-dimensional formulation used in previous studies.[11] Despite being inviscid, steady, and incompressible, Culick's profile was rotational and could satisfy the fundamental boundary conditions associated with an internal-burning cylindrical grain.  Unlike its predecessor, it could now satisfy the vital no-slip condition at the wall and insure that gases are ejected perpendicularly to the burning surface.  It also matched Taylor's solution[1] obtained in an unrelated problem.  The latter involved running watery suspensions of fibers over porous sheets through which the fluid could be drained to form paper.  Both solutions were exact in the limit of an infinitesimally small viscosity or of an infinitely large injection velocity.  Culick's solution was convenient, simple, and reasonably accurate over a range of Reynolds numbers exceeding 200.  It also lent itself to both numerical[12] and experimental verifications by Dunlap et al.[13] and Yamada, Goto and Ishikawa.[14] Aside from a small region near the head-end of the chamber, Culick's profile appeared to adequately represent the viscous flow solution measured in a porous tube.  Culick's inviscid profile has also been used as the basis to investigate the onset of hydrodynamic instability by Varapaev and Yagodkin,[15] and, more recently, by Casalis, Avalon and Pineau.[16] While the former carried out a preliminary numerical study of the linear stability of Culick's solution, the latter employed an original, analytical approach the results of which could be compared to experimental measurements.  Other workers have also investigated the onset of turbulence and its evolution from the mean flow.  To name a few, one may enumerate Beddini and Roberts,[17] Sabnis, Gibeling and McDonald,[18] Tissier, Godfrey and Jacquemin,[19] Roh, Tseng and Yang,[20] and Apte and Yang.[21] In addition to its pertinence to studies of hydrodynamic instability, the mean-flow profile has also been influential in the development of the oscillatory flow component that is used to describe the vortico-acoustic wave motion inside rocket motors.

In fact, it may be safely stated that the oscillatory flow analogue was pioneered by Flandro[22] who pointed out the shortcomings of using a one-dimensional plane wave solution.[23] As a quick remedy, Flandro presented an analytical solution for the oscillatory field that accounted for the presence of solid boundaries.[24] His early model was two-dimensional only artificially since it ignored the downstream convection of unsteady vorticity and the spatial depreciation of Culick's radial velocity.  It was, however, valid in a small region above the burning surface wherein important mechanisms were present.  An asymptotic solution by Majdalani and Van Moorhem ensued.[25,26] The latter employed the exact Culick profile but still was unable to incorporate the axial dependency.

Following Flandro's footsteps, Kirkköprü, Zhao and Kassoy[27] attempted to use multiple scales, which were successfully employed by Majdalani,[28] in order to analyze the developing transient flow that preceded the inception of steady-state oscillations.  Kirkköprü and co-workers provided a crude flow approximation that was based on a quasi-analytical approach and two conjectured scales found by intuition.  Being the product of guesswork, these scales were different from the uniformly valid transformations that were prescribed by the problem's solvability condition and the principle of least singular behavior.  As such, they differed from those derived and verified by Majdalani,[29] and Majdalani and Roh.[30]

Flandro[31] later presented an inviscid solution that fully retained Culick's profile and the correct spatial dependency.  Shortly thereafter, Flandro obtained a multidimensional solution that incorporated viscosity.[32] A practically equivalent solution based on multiple-scales was furnished by Majdalani and Van Moorhem.[25] Majdalani and Van Moorhem[33] would later demonstrate the agreement between both contemporaneous solutions and full numerical simulations.  Their results were also found to reasonably agree with test measurements

acquired by Barron, Van Moorhem and Majdalani,[34] Brown *et al.*[35] and Dunlap *et al.*[36] The multiple-scale solution was also able to elucidate the nature of the acoustic boundary layer that, until then, had been the subject of controversy in the propulsion community.[37]

The slab-rocket analogue has also been analyzed by Majdalani and Roh[30] and, for an arbitrary mean-flow profile, by Majdalani,[38] and Majdalani and Van Moorhem.[39] Therein, a fully rotational and viscous representation for the oscillatory field has been accomplished. Being of higher-order and expressible in a general conceptual format, the newly developed representation offers the advantage of accommodating any valid mean-flow profile. Inasmuch as the higher level of precision achieved in these recent studies remains limited by the accuracy of the inviscid mean-flow solution, the motivation arises for a higher-order approximation that can be consistent with the unsteady flow details.

In addition to the fact that a more comprehensive mean-flow solution can a) improve the accuracy of existing time-dependent models, b) provide a better platform to investigate linear hydrodynamic stability, and c) enhance our internal flow predictive capabilities, it also serves to extend the range over which current models apply. In fact, according to Yuan[40] (cf. p. 267), there are numerous problems of real interest that exhibit crossflow Reynolds numbers that can be as low as 10.

Due to the foregoing reasons, as for so much else, it is the purpose of this article to obtain a more general mean-flow solution that not only satisfies the basic boundary conditions, but is also capable of fully incorporating viscous forces and wall regression. A direct consequence of such a higher-order mean-flow solution is the attainment of a total internal flow solution in general form that is consistently rotational and viscous in both its mean and oscillatory components. Furthermore, the resulting solutions should be useful over a broader range of physical applications. They become especially suitable to model motors with high burning rate propellants such as those being developed for high-acceleration interceptor vehicles. Aside from its practical usefulness, this work serves as an extension to the planar solution presented recently by Majdalani[38] and Zhou and Majdalani.[41]

The article can be divided into two parts. In the first, we apply Goto and Uchida's approach[42] to provide the clear steps leading to the reduction of the Navier-Stokes system into a single, exact, similarity solution. The procedure involves a spatial transformation that presumes a linearly varying axial velocity and a temporal transformation that is granted by a constant (dimensionless) regression ratio.
In the second part, we follow Yuan and Finkelstein[43] and Terrill[12] in perturbing the resulting fourth-order nonlinear equation. In the process, we follow a similar procedure to that used by Zhou and Majdalani[41] who have recently obtained an expression for the mean-flow field in a slab rocket motor. As such, we find it necessary to apply a quadruple variation of parameters. Subsequently, a higher-order mean-flow approximation is obtained for the velocity, pressure and shear stress distributions. These are described in addition to limiting process verifications that we have employed to validate our solutions. Our results clearly indicate the existence of a range over which the inviscid approximation deteriorates. By the same token, we demonstrate the suitability of Culick's profile over a substantial range of conditions arising in solid rocket motors. A numerical comparison that is identical to that described by Zhou and Majdalani[41] is also carried out but will be omitted here for lack of novelty.

## II.    Mathematical Model

The internal-burning cylindrical grain model of a solid rocket motor is idealized as a long tube with one end closed. Furthermore, the circumferential walls are assumed to be sufficiently permeable to allow the radial influx of a secondary fluid. The radially incoming stream turns and merges into the primary axial flow while heading downstream. As the circumferential walls expand at a speed equal to $\dot{a}$, the head-end is assumed to be sufficiently compliant to stretch in the radial direction while remaining perpendicular to the tube's axis at any radius $a(t)$. As shown in Fig. 1, a coordinate system can be chosen in such a way to take advantage of the problem's axisymmetry. With this choice, the incompressible mass and momentum conservation equations may be written as

$$\frac{\partial(\overline{r u_z})}{\partial \overline{z}} + \frac{\partial(\overline{r u_r})}{\partial \overline{r}} = 0 \tag{1}$$

$$\frac{\partial \overline{u}_z}{\partial t} + \overline{u}_z \frac{\partial \overline{u}_z}{\partial \overline{z}} + \overline{u}_r \frac{\partial \overline{u}_z}{\partial \overline{r}} = -\frac{1}{\rho}\frac{\partial \overline{p}}{\partial \overline{z}} + \nu\left[\frac{\partial^2 \overline{u}_z}{\partial \overline{z}^2}\right.$$
$$\left. + \frac{1}{\overline{r}}\frac{\partial}{\partial \overline{r}}\left(\overline{r}\frac{\partial \overline{u}_z}{\partial \overline{r}}\right)\right] \tag{2}$$

$$\frac{\partial \overline{u}_r}{\partial t} + \overline{u}_z \frac{\partial \overline{u}_r}{\partial \overline{z}} + \overline{u}_r \frac{\partial \overline{u}_r}{\partial \overline{r}} = -\frac{1}{\rho}\frac{\partial \overline{p}}{\partial \overline{r}} + \nu\left[\frac{\partial^2 \overline{u}_r}{\partial \overline{z}^2}\right.$$
$$\left. + \frac{\partial}{\partial \overline{r}}\left(\frac{1}{\overline{r}}\frac{\partial(\overline{r u_r})}{\partial \overline{r}}\right)\right] \tag{3}$$

where variables have their usual significance or as given in the Nomenclature. Boundary conditions are:

$$\overline{r} = a(t), \overline{u}_z = 0,\ \overline{u}_r = -V \tag{4}$$

$$\overline{r} = 0, \frac{\partial \overline{u}_z}{\partial r} = 0,\ \overline{u}_r = 0 \tag{5}$$

and  $\overline{z} = 0, \overline{u}_z = 0$ $\tag{6}$

where $V$ is the absolute velocity at the wall.

## A. Basic Assumptions

Equations (1)–(6) are written under the implicit assumptions that:
1) The bulk flow is incompressible and isothermal.
2) Body forces are absent.
3) The kinematic viscosity $\nu$ is constant.
4) The fluid enters the tube at a uniform velocity $V$.
5) Swirling effects can be ignored.
6) The azimuthal component of velocity is zero.
7) Conditions preclude the onset of turbulence.
8) No heat is transferred to the gas.

## B. The General Mass Balance Requirement

Consider in Fig. 1 a control volume $\vartheta$ extending from the head-end to an arbitrary position $\overline{z}$. The average axial flow velocity $\overline{u}_m(\overline{z},t)$ at a given cross section $A_c(\overline{z})$ can be determined from

$$\overline{u}_m(\overline{z},t) = \frac{1}{A_c}\int_{A_c} \boldsymbol{u} \cdot \mathrm{d}\boldsymbol{A} \tag{7}$$

where $\boldsymbol{u}$ is the local axial velocity and $\mathrm{d}\boldsymbol{A} = \boldsymbol{n}\,\mathrm{d}A$ is the element of area whose normal unit vector is axial. Since $A_c = \pi a^2$ and $A_b(\overline{z}) = 2\pi a \overline{z}$ denotes the volume's circumferential area, conservation of mass across $\vartheta$ necessitates that

$$\frac{\partial}{\partial t}\int_{\vartheta}\rho\,\mathrm{d}\vartheta + \rho A_b V_b - \int_{A_c}\rho\boldsymbol{u}\cdot\mathrm{d}\boldsymbol{A} = 0 \tag{8}$$

where $\mathrm{d}\vartheta = A_c\,\mathrm{d}\overline{z}$ and $V_b$ is the fluid velocity with respect to the wall. Recalling that the flow is incompressible, one may substitute Eq. (7) into Eq. (8), and then integrate from $0$ to $\overline{z}$. After some rearrangement, one obtains

$$\overline{u}_m = \frac{A_b}{A_c}V_b - \frac{\overline{z}}{A_c}\frac{\partial A_c}{\partial t} = 2\frac{\overline{z}}{a}(V_b - \dot{a}) = 2\frac{\overline{z}}{a}V \tag{9}$$

where $V = V_b - \dot{a}$ is the absolute inflow velocity with respect to an inertial reference frame. Equation (9) indicates that the mean velocity is proportional to the axial coordinate and suggests the possibility of a similarity transformation.

## C. Mass Balance at the Propellant Surface

In problems for which fluid injection and wall motion are controlled by separate processes, $V_b$ and $\dot{a}$ are independent parameters. In solid propellant rocket motors, however, the relative velocity of the gas with
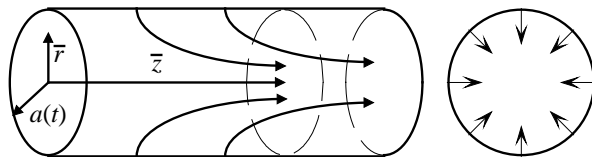


**Fig. 1 Coordinate system for a cylindrical motor with regressing inner walls.**

respect to the regressing walls and the speed of wall regression are related. To find this relation, one must recognize that, in any given time interval, the mass of propellant burned must equal the mass of gases ejected into the chamber. Since $A_b$ denotes the burning surface in a solid propellant motor (or the sublimating surface in a cold-flow simulation of the burning process,[34,44,45]) conservation of mass at the solid-gas interface requires that $\rho A_b V_b = \rho_s A_b \dot{a}$. The gas velocity with respect to the wall becomes

$$V_b = (\rho_s / \rho)\dot{a} \tag{10}$$

where $\rho_s$ is the density of the solid phase (before solid propellant pyrolysis or hard-wall sublimation). From Eq. (10), the absolute velocity can be seen to be

$$V = (\rho_s/\rho - 1)\dot{a} = A\dot{a} \tag{11}$$

where $A = \rho_s/\rho - 1$ is the wall permeance or injection coefficient.[42] Since $A \equiv V/\dot{a}$, it is a measure of wall permeability. In rocket motors, $\rho_s \sim 2000$ kg.m$^{-3}$, $\rho \sim 20$ kg.m$^{-3}$, and $A \sim 100$. At the other extreme, one may envisage a cold-flow experiment in which the walls are allowed to expand in the absence of forced injection (e.g., for nonreactive walls). For such a hypothetical case, $V_b$ will be zero, $V = -\dot{a}$, $A = -1$, and the flow reverses to suction due to pure expansion of the inert walls.

## D. Similarity in Space

The condition of incompressibility enables us to use the stream function $\overline{\psi}$ and reduce the Navier-Stokes equations. Starting with

$$\overline{u}_z = \frac{1}{r}\frac{\partial\overline{\psi}}{\partial r} \quad \overline{u}_r = -\frac{1}{r}\frac{\partial\overline{\psi}}{\partial\overline{z}} \tag{12}$$

one may follow Goto and Uchida[42] and write the stream function in a form that is consistent with mass conservation; namely, a form that can lead to a linear $\overline{z}$-variation in the axial velocity. We thus let

$$\overline{\psi} = \nu\overline{z}\overline{F}(r,t) \ ; \quad r = \frac{\overline{r}}{a(t)} \tag{13}$$

In terms of $\overline{F}$, the axial and radial velocities become

$$\overline{u}_z = \frac{1}{r}\frac{\partial\overline{\psi}}{\partial\overline{r}} = \frac{1}{r}\frac{\partial(\nu\overline{z}\overline{F})}{\partial\overline{r}} = \frac{\nu\overline{z}}{a^2}\frac{1}{r}\frac{\partial\overline{F}}{\partial r} \tag{14}$$

$$\overline{u}_r = -\frac{1}{r}\frac{\partial\overline{\psi}}{\partial\overline{z}} = -\frac{1}{r}\frac{\partial(\nu\overline{z}\overline{F})}{\partial\overline{z}} = -\frac{\nu\overline{F}}{ar} \tag{15}$$

Since the radial velocity is independent of $\overline{z}$, vorticity simplifies into

$$\Omega = |\nabla\times\boldsymbol{u}| = -\frac{\partial\overline{u}_z}{\partial\overline{r}} \tag{16}$$

The vorticity transport equation becomes,

$$\boldsymbol{\Omega}_t + \boldsymbol{u}\cdot\nabla\boldsymbol{\Omega} = \nu\nabla^2\boldsymbol{\Omega} \tag{17}$$

or
$$\frac{\partial}{\partial \overline{r}}\left(\frac{\partial \overline{u}_z}{\partial t}\right)+\frac{\partial}{\partial \overline{r}}\left(\overline{u}_z \frac{\partial \overline{u}_z}{\partial \overline{z}}\right)+\frac{\partial}{\partial \overline{r}}\left(\overline{u}_r \frac{\partial \overline{u}_z}{\partial \overline{r}}\right)$$
$$-\nu\frac{\partial}{\partial \overline{r}}\left[\frac{1}{\overline{r}}\frac{\partial}{\partial \overline{r}}\left(\overline{r}\frac{\partial \overline{u}_z}{\partial \overline{r}}\right)\right]=0 \qquad (18)$$

In order to apply the transformations given by Eqs. (13)–(15), partial derivatives must be carefully evaluated. These involve:

$$\frac{\partial \overline{u}_z}{\partial t}=\frac{\nu\overline{z}}{a^2}\frac{\partial}{\partial t}\left(\frac{\overline{F}_r}{r}\right)-\frac{2\nu\overline{z}}{a^3}\frac{\overline{F}_r}{r}\dot{a} \qquad (19)$$

$$\frac{\partial \overline{u}_z}{\partial \overline{r}}=\frac{\nu\overline{z}}{a^3}\frac{\partial}{\partial r}\left(\frac{\overline{F}_r}{r}\right),\quad \frac{\partial \overline{u}_z}{\partial \overline{z}}=\frac{\nu}{a^2}\frac{\overline{F}_r}{r} \qquad (20)$$

$$\overline{u}_r\frac{\partial \overline{u}_z}{\partial \overline{r}}=-\frac{\nu^2\overline{z}}{a^4}\frac{\overline{F}}{r}\frac{\partial}{\partial r}\left(\frac{\overline{F}_r}{r}\right),\quad \overline{u}_z\frac{\partial \overline{u}_z}{\partial \overline{z}}=\frac{\nu^2\overline{z}}{a^4}\left(\frac{\overline{F}_r}{r}\right)^2 \qquad (21)$$

and,
$$\frac{1}{\overline{r}}\frac{\partial}{\partial \overline{r}}\left(\overline{r}\frac{\partial \overline{u}_z}{\partial \overline{r}}\right)=\frac{\nu\overline{z}}{a^4}\frac{1}{r}\frac{\partial}{\partial r}\left[r\frac{\partial}{\partial r}\left(\frac{\overline{F}_r}{r}\right)\right] \qquad (22)$$

## E.  The Reduced Navier-Stokes Equation

Substituting Eqs. (19)—(22) in Eq. (18) yields
$$\left\{(-\nu\overline{z}/a^3)(\overline{F}_{rt}/r)+(\dot{a}\nu\overline{z}r/a^4)(\overline{F}_r/r)_r\right.$$
$$+(2\nu\dot{a}/a^4)(\overline{z}/r)\overline{F}_r-(\nu^2\overline{z}/a^5)(\overline{F}_r/r)^2$$
$$+(\nu^2\overline{z}/a^5)(\overline{F}/r)(\overline{F}_r/r)_r+(1/r)(\overline{F}_r/r)_r$$
$$\left.+(\overline{F}_r/r)_{rr}\right\}_r=0 \qquad (23)$$

Next, one introduces the dimensionless expansion ratio
$$\alpha(t)\equiv \dot{a}a/\nu \qquad (24)$$

Clearly, $\alpha$ is a Reynolds number based on the expansion speed of the walls. Inserting Eq. (24) into Eq. (23) renders, after some algebra,
$$\left\{\left(\overline{F}_r/r\right)_{rr}+\left[(1+\overline{F})/r+\alpha r\right]\left(\overline{F}_r/r\right)_r\right.$$
$$\left.-\left(\overline{F}_r/r-2\alpha\right)\overline{F}/r-(a^2/\nu)(\overline{F}_{rt}/r)\right\}_r=0 \qquad (25)$$

whose boundary conditions may be obtained from Eqs. (4)–(6). These translate into
$$\overline{F}_r/r=0,\ \overline{F}/r=R;\ \text{at } r=1 \qquad (26)$$
$$\left(\overline{F}_r/r\right)_r=0,\ \overline{F}/r=0;\ \text{at } r=0 \qquad (27)$$

where $R\equiv Va/\nu$ is the Reynolds number based on the absolute injection velocity. Equation (25) embodies a generalization of Yuan and Finkelsetein's[43] and is consistent with that solved numerically by Goto and Uchida.[42] Note that $R$ and $\alpha$ are generally unrelated. However, for cases involving propellant combustion or solid phase sublimation, Eq. (11) can be multiplied by $a/\nu$ to obtain
$$Va/\nu=(\rho_s/\rho-1)\dot{a}a/\nu,\ \text{or } R=A\alpha \qquad (28)$$

Under such conditions, $R$ and $\alpha$ become intimately related by the solid-to-gas density ratio. For illustrative purposes, a range of physical parameters corresponding to solid propellants is taken from Sutton[46] and compiled

in Table 1 (cf. pp. 370, 375, 418, and 435). We note that data regarding viscosity is based on the Lucas model which is applicable at high temperatures and pressures.[47] We also note that the maximum regression speed is taken from a recent work by Beckstead.[48]

## F.  Similarity in Time

In order to make further headway towards a more manageable equation, we assume self-similarity in time that can be reasonably justified in practice. Using the same argument presented by Uchida and Aoki,[49] we first apply the transformation $\overline{F}(r,t)\rightarrow \overline{F}\left[r,\alpha(t)\right]$ and then define $\alpha$ to be invariant in time. To realize this condition, $\alpha$ must be specified by its initial value, namely
$$\alpha=\dot{a}a/\nu=\dot{a}_0 a_0/\nu \qquad (29)$$
where $a_0$ and $\dot{a}_0$ represent the initial radius and regression rate. The ensuing similarity transformation can be arrived at by integrating Eq. (29) with respect to time. One obtains
$$a(t)=a_0\sqrt{1+2\nu\alpha t a_0^{-2}} \qquad (30)$$
Since $a=\alpha\nu/\dot{a}$, Eq. (30) indicates that
$$\dot{a}(t)/\dot{a}_0=\left(1+2\nu\alpha a_0^{-2}t\right)^{-\frac{1}{2}}\cong 1-\nu\alpha a_0^{-2}t \qquad (31)$$

From a physical standpoint, the similarity in time corresponds to slowly decelerating walls. In a solid propellant motor, such a condition can be associated with a progressive, neutral, or regressive thrust since the burn area always increases with the passage of time. Neutral or regressive thrust traces can be modeled, for example, when the slow reduction in $\dot{a}$ as time progresses is sufficient to exactly or more than offset the increased mass influx resulting from the constantly increasing $A_b$. Note that when $A$ is fixed, Eq. (11) suggests that $V(t)/V(0)$ will vary according to Eq. (31) as well.

## G.  A Self-Similarity Solution in Time and Space

Under the auspices of a time-invariant $\alpha$, we find it useful to define
$$F\equiv \overline{F}/R\ ;\ \eta\equiv \tfrac{1}{2}r^2\ ;\ \text{and } \varepsilon\equiv 1/R \qquad (32)$$
Backward substitution into Eq. (25) yields, at length,

Table 1.  Range of parameters for SRMs

| Variables/Parameters | Symbol | Range | Units |
|---|---|---|---|
| Radius of motor grain | $a$ | 0.005 – 3.5 | m |
| Grain density | $\rho_s$ | 1,500 – 2,500 | kg/m³ |
| Gas density | $\rho$ | 10 – 20 | kg/m³ |
| Kinematic viscosity | $\nu$ | $10^{-6} - 10^{-5}$ | m²/s |
| Grain burn rate | $\dot{a}$ | 0.0005 – 0.1 | m/s |
| Gas injection velocity | $V_b$ | 0.0075 – 10 | m/s |
| Expansion ratio | $\alpha$ | 0.125 – 35,000 | |
| Injection Reynolds no. | $R$ | 35 – 3,300,000 | |

$$\varepsilon\left[2\eta\frac{d^4F}{d\eta^4}+(2\alpha\eta+3)\frac{d^3F}{d\eta^3}+4\alpha\frac{d^2F}{d\eta^2}\right]$$
$$+F\frac{d^3F}{d\eta^3}-\frac{dF}{d\eta}\frac{d^2F}{d\eta^2}=0 \qquad (33)$$

which is subject to

$$\frac{dF\left(\tfrac{1}{2}\right)}{d\eta}=0;\ F\left(\tfrac{1}{2}\right)=1;\ F(0)=0 \qquad (34)$$

$$\lim_{\eta\to 0}\sqrt{2\eta}\frac{d^2F}{d\eta^2}=0 \qquad (35)$$

Next, we solve this set using asymptotic tools.

## III. Analytical Solution

According to Terrill,[12,50] a regular perturbation expansion is expected to hold true for moderate to large injection Reynolds numbers everywhere except near the core where a special treatment is necessary. To start, we expand the solution via $F=F_0+\varepsilon F_1+O(\varepsilon^2)$ and substitute back into Eq. (33). At zeroth order, a basic solution is obtained, namely,

$$F_0\frac{d^3F_0}{d\eta^3}-\frac{dF_0}{d\eta}\frac{d^2F_0}{d\eta^2}=0 \qquad (36)$$

The solution to this equation can be guessed to be $F_0=\sin(\pi\eta)$. Defining $\theta\equiv\pi\eta$, the first-order equation of $O(\varepsilon)$ may now be written as

$$\sin\theta\frac{d^3F_1}{d\theta^3}-\cos\theta\frac{d^2F_1}{d\theta^2}+\sin\theta\frac{dF_1}{d\theta}-\cos\theta F_1$$
$$=\ (2\alpha\frac{\theta}{\pi}+3)\cos\theta+\frac{4\alpha}{\pi}\sin\theta-2\theta\sin\theta \qquad (37)$$

### A. Variation of Parameters

In order to make headway, one must guess that a partial solution must be $F_{1h}=\cos\theta$. The variation of parameters approach can then be used to determine the correction multiplier based on $F_{1h}=C(\theta)\cos\theta$. Thus, backward substitution into the homogeneous part of Eq. (37) yields

$$C'''\sin\theta\cos\theta-2C''\sin^2\theta-C''=0 \qquad (38)$$

wherefrom $\quad C(\theta)=K_0\tan\theta+K_1\theta+K_2 \qquad (39)$

The complete homogeneous solution becomes

$$F_{1h}=K_0\sin\theta+K_1\theta\cos\theta+K_2\cos\theta \qquad (40)$$

where $K_0$, $K_1$ and $K_2$ are yet to be determined. The method of variation of parameters is applied once more by turning the three integration constants into undetermined functions. We thus set

$$F_1(\theta)=K_0(\theta)\sin\theta+K_1(\theta)\theta\cos\theta+K_2(\theta)\cos\theta \qquad (41)$$

Substituting the above into Eq. (37) leads to

$$K_0'\sin\theta+K_1'\theta\cos\theta+K_2'\cos\theta=0 \qquad (42)$$

$$K_0'\cos\theta+K_1'(\cos\theta-\theta\sin\theta)-K_2'\sin\theta=0 \qquad (43)$$

$$K_0'\sin^2\theta+K_1'(2\sin^2\theta+\theta\cos\theta\sin\theta)+K_2'\cos\theta\sin\theta$$
$$=-[(2\alpha/\pi)\theta+3]\cos\theta+(4\alpha/\pi)\sin\theta-2\theta\sin\theta \qquad (44)$$

Solving Eqs. (42)—(44) simultaneously enables us to determine the variable coefficients. These are found to be

$$K_0=(\alpha/\pi)\left[-\theta\csc\theta+3\ln\tan\tfrac{1}{2}\theta+(\cos\theta-\theta\sin\theta)\right]$$
$$-\tfrac{3}{2}\csc\theta-\tfrac{1}{2}\sin\theta-\theta\cos\theta-S(\theta)+C_0 \qquad (45)$$

$$K_1=(\alpha/\pi)\left(\theta\csc\theta-3\ln\tan\tfrac{1}{2}\theta\right)+\tfrac{3}{2}\csc\theta$$
$$+S(\theta)+C_1 \qquad (46)$$

$$K_2=(\alpha/\pi)\left[3S(\theta)-\theta\cos\theta-\sin\theta-\theta^2\csc\theta\right]$$
$$-\tfrac{1}{2}\cos\theta+\theta\sin\theta-\tfrac{3}{2}\theta\csc\theta-S_1(\theta)+C_2 \qquad (47)$$

where $S(\theta)=\int_0^\theta\phi\csc\phi\,d\phi,\ S_1(\theta)=\int_0^\theta\phi^2\csc\phi\,d\phi \quad (48)$

In series form, these integrals become

$$S(x)=x+\sum_{k=1}^\infty\frac{2}{\pi^{2k}}\left(\sum_{n=1}^\infty\frac{1}{n^{2k}}\right)\frac{\left(1-2^{1-2k}\right)}{(2k+1)}x^{2k+1} \qquad (49)$$

$$S_1(x)=\frac{x^2}{2}+\sum_{k=1}^\infty\frac{1}{\pi^{2k}}\left(\sum_{n=1}^\infty\frac{1}{n^{2k}}\right)\frac{\left(1-2^{1-2k}\right)}{(k+1)}x^{2k+2} \qquad (50)$$

### B. First-order Solution

To recapitulate, we recall that $\theta=\pi\eta$ and express the basic and first order solutions for $F$. These are

$$F_0=\sin\theta \qquad (51)$$

$$F_1=(\alpha/\pi)\left[3\ln\tan\tfrac{1}{2}\theta(\sin\theta-\theta\cos\theta)-2\theta\right]$$
$$-2+(\theta\cos\theta-\sin\theta)S(\theta)$$
$$+\left[3(\alpha/\pi)S(\theta)-S_1(\theta)\right]\cos\theta$$
$$+C_0\theta\cos\theta+C_1\sin\theta+C_2\cos\theta \qquad (52)$$

The remaining constants can be determined from the boundary conditions given by Eqs. (34)–(35). One finds

$$C_0=-(4/\pi)+\left(2\alpha/\pi^2-1\right)-S\left(\tfrac{1}{2}\pi\right)\left(6\alpha/\pi^2+1\right)$$
$$+(2/\pi)S_1\left(\tfrac{1}{2}\pi\right) \qquad (53)$$

$$C_1=\left[\alpha+2+S\left(\tfrac{1}{2}\pi\right)\right],\ C_2=2 \qquad (54)$$

At this juncture, the axial and radial components of velocity and pressure can be readily evaluated. One finds Taylor's,[1] Culick's,[10] or Yuan and Finkelstein's[43] to be recoverable from Eqs. (51)–(54).

To avoid singularities at the core, however, we resort to $\eta$ as our independent coordinate for calculations and plots. To maintain generality, we present variables in the following dimensionless form

$$z=\frac{\overline{z}}{a},\ \psi=\frac{\overline{\psi}}{a^2V}=zF,\ p=\frac{\overline{p}}{\rho V^2} \qquad (55)$$

$$u_r = \frac{\overline{u}_r}{V} = -\frac{F}{r} = -\frac{F}{\sqrt{2\eta}} \qquad (56)$$

$$u_z = \frac{\overline{u}_z}{V} = \frac{z}{r}\frac{\partial F}{\partial r} = z\frac{\mathrm{d}F}{\mathrm{d}\eta}, \quad u_{\mathrm{m}} = \frac{\overline{u}_{\mathrm{m}}}{V} = 2z \qquad (57)$$

Pursuant to these choices, the axial velocity normalized by the mean axial velocity becomes, at any position,

$$u_z / u_{\mathrm{m}} = \tfrac{1}{2}\mathrm{d}F / \mathrm{d}\eta \qquad (58)$$

In like fashion, the normalized radial pressure loss measured from the core can be found. Starting with

$$\frac{\mathrm{d}P}{\mathrm{d}\eta} = -\frac{\mathrm{d}}{\mathrm{d}\eta}\left[\varepsilon\frac{\mathrm{d}F}{\mathrm{d}\eta} + \alpha\varepsilon F + \left(\frac{F}{\eta}\right)^2\right] \qquad (59)$$

one may integrate from the core to any radial location. The resulting drop is found to be

$$\Delta p_r \equiv -\left[p(\eta, z) - p(0, z)\right]$$

$$= \varepsilon\frac{\mathrm{d}F}{\mathrm{d}\eta} + \alpha\varepsilon F + \frac{1}{\eta}\left(\frac{F}{2}\right)^2 - \varepsilon\frac{\mathrm{d}F(0)}{\mathrm{d}\eta} \qquad (60)$$

Similarly, the axial pressure drop measured from the head-end becomes

$$\Delta p_z \equiv p(\eta, z) - p(\eta, 0)$$

$$= \tfrac{1}{2}z^2\left[\varepsilon\left(-\frac{\mathrm{d}^2 F}{\mathrm{d}\eta^2} + \frac{1}{2\eta}\frac{\mathrm{d}F}{\mathrm{d}\eta} + 2\eta\frac{\mathrm{d}^3 F}{\mathrm{d}\eta^3}\right.\right.$$

$$\left.\left. + \alpha\frac{\mathrm{d}F}{\mathrm{d}\eta} + 2\alpha\eta\frac{\mathrm{d}^2 F}{\mathrm{d}\eta^2}\right) - \left(\frac{\mathrm{d}F}{\mathrm{d}\eta}\right)^2 - \frac{F}{\eta}\frac{\mathrm{d}F}{\mathrm{d}\eta} + F\frac{\mathrm{d}F}{\mathrm{d}\eta}\right] \qquad (61)$$

Finally, the shear stress may be determined from Newton's law for viscosity. One finds

$$\tau = \frac{\overline{\tau}}{\rho V^2} = 2\varepsilon\eta z\frac{\mathrm{d}^2 F}{\mathrm{d}\eta^2} \qquad (62)$$

which, at the wall, gives

$$\tau_{\mathrm{b}} = \varepsilon z\frac{\mathrm{d}^2 F}{\mathrm{d}\eta^2}(\tfrac{1}{2}) \qquad (63)$$

## IV.   Results

To gain better understanding of the effects of viscosity and wall regression on the flow character, the main flow attributes are described over different ranges of the control parameters. This description is hoped to aid in interpreting the significance of the higher-order formulation and gain more insight into the physics of the problem. This will be accomplished by examining the behavior of flow streamlines, axial and radial velocities, axial and radial pressure distributions, and shearing stress at the wall.

### A.   Streamlines

In Fig. 2, streamline patterns are shown for two widely dissimilar values of the Reynolds number either a) with and b) without wall regression. From Fig. 2a, it may be inferred that, in the absence of wall motion,
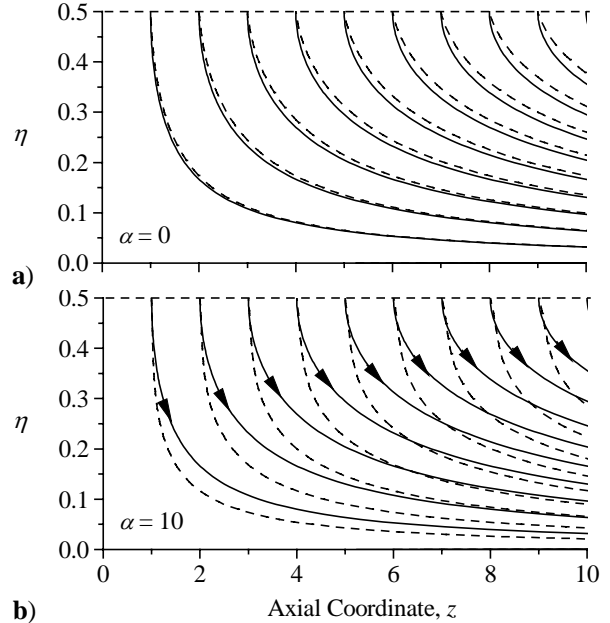


**Fig. 2 Influence of the regression rate on the streamlines for ‑ ‑ ‑ ‑ $R = 10$, —— $R = 1000$.**

only slight differences in streamline curvatures are noticed near the head-end despite the two orders of magnitude separating the Reynolds numbers. Differences in streamline curvatures and, hence, the flow turning speed, become more appreciable when moving downstream. The effects of viscosity are, therefore, more significant in the downstream portions of the tube. Furthermore, as the Reynolds number is decreased from 1000 to 10, the viscous decay of the radial component of the velocity takes place more rapidly than the slower decay in the axial direction. As a result, the flow turning speed is increased, leading to a sharper streamline curvature near the walls.

Figure 2b, on the other hand, indicates that lower Reynolds number flows are more sensitive to changes in wall regression than inviscid flows. As it can be inferred by inspection of Eq. (33), the determining factor appears to be $\alpha / R$ or $1 / A$. The smaller this factor is, the less sensitive the flow will be, and more closely will it resemble the inviscid analogue, especially near the head-end. Far downstream, however, the otherwise negligible discrepancies between viscous and inviscid flows with stationary or expanding walls become magnified due to their cumulative nature while crossing the length of the tube. Figure 2b also indicates that the effect of fast wall expansion is to reduce the flow turning speed (e.g., for $R = 10$). The higher the expansion speed, the longer will the radial velocity be large in comparison to its axial counterpart while approaching the core. The radius of curvature of an incoming streamline is thus increased with $\dot{a}$. A purely hypothetical case arises,

for instance, when the walls expand at nearly the same speed as that of the fluid entering the tube (i.e., $\dot{a} = V_b$). Under such conditions, the expansion process will offset the effect of injection to the point that streamlines will exhibit an infinite radius of curvature and remain perpendicular to the walls. If this happens, the flow turning process will be delayed indefinitely.
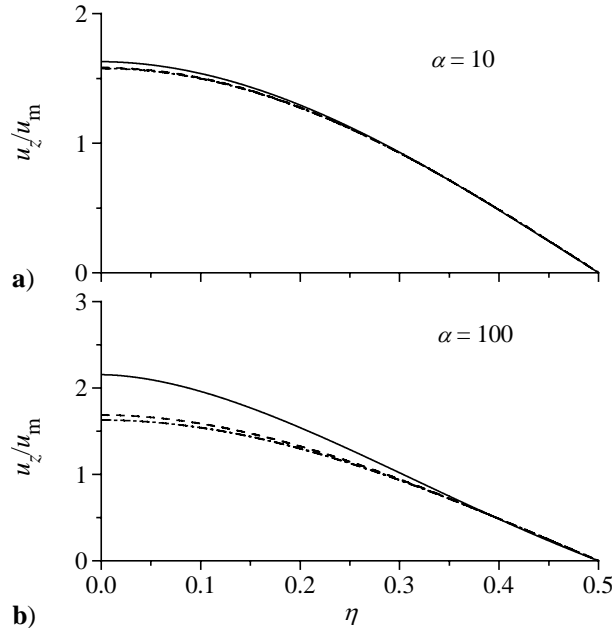


**Fig. 3 Influence of the regression rate on the axial velocity for —— $R = 100$, - - - - $R = 500$, -·-·-·- $R = 1000$.**
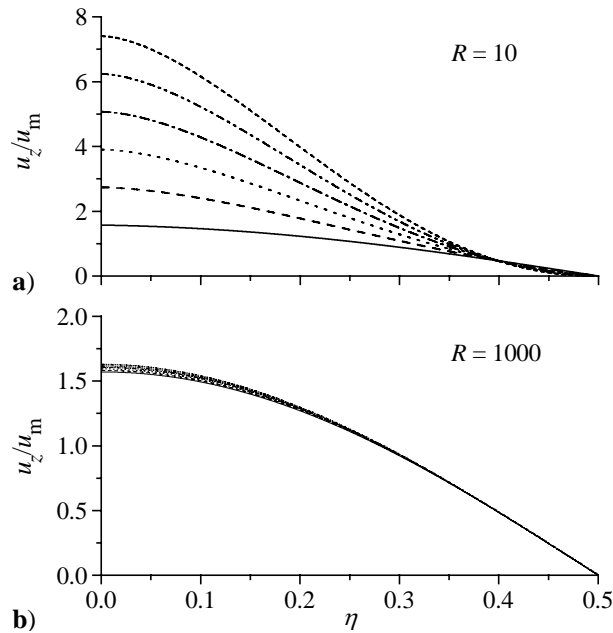


**Fig. 4 Sensitivity of the axial velocity to the regression rate at a) moderate and b) large injection Reynolds numbers. The regression rate is —— 0, - - - - 20, ······ 40, -·-·-· 60, -··-··- 80, ------- 100.**

**B. Axial Velocity**

Figures 3 and 4 illustrate the behavior of axial velocity profiles, normalized by their mean values $u_m$, over a range of $R$ and $\alpha$. Similar trends to those associated with streamline curvatures may be observed. For instance, a greater sensitivity to wall regression is observed at smaller values of $R$. Figure 3 indicates that, as $\alpha$ changes from a) 10 to b) 100, the centerline velocity increases from 1.63 to 2.15 times the average velocity for a Reynolds number of 100. This 32% increase in the centerline-to-mean velocity ratio is quite significant by comparison to the 7% and 3% increases observed at $R = 500$ and $1000$, respectively. It is interesting to note that, when the walls are made permeable and allowed to expand, the 2.15 overshoot over $u_m$ in Fig. 3b exceeds the factor of 2 associated with a fully-developed Poiseuille flow in a tube.

For fixed $R$, the regression rate is now varied by equal increments in Fig. 4 over the range 0 to 100. In Fig. 4a, a significant variation in the centerline-to-mean velocity ratio is observed ranging from 1.57 to 7.41 as $\alpha$ is increased from 0 to 100. This 372% speed augmentation at the centerline can be achieved or even exceeded when $\alpha$ is prescribed in a manner to be of the same order or larger than $R$. When this is no longer the case, such as in Fig. 4b (where $R = 1000$), the mean-flow overshoot at the centerline is increased only from 1.57 to 1.63; this marks a mere 4% magnification, for the same variation in $\alpha$. We conclude that the centerline-to-mean velocity overshoot is sensitive to the relative expansion speed and therefore commensurate with the size of $\alpha / R$. For sufficiently small $\alpha / R$, the centerline-to-mean velocity ratio asymptotes to 1.57 or $\frac{1}{2}\pi$. This ratio is due to the mean velocity being $2z$ according to Eq. (57), and to the inviscid axial velocity being $u_z(r, z) = \pi z \cos(\frac{1}{2}\pi r^2) = \pi z$ at the centerline. It also coincides with the center-to-mean velocity ratio in a planar channel with porous walls wherein $u_z(x, y) = \frac{1}{2}\pi x \cos(\frac{1}{2}\pi y) = \frac{1}{2}\pi x$ and the mean velocity is simply $x$.[39]

**C. Radial Velocity**

The radial velocity is described in Fig. 5 for three different values of the relative regression rate $\alpha / R$. At the outset, two interesting phenomena are observed. The first corresponds to the existence of a point on the interval $0 < \eta < \frac{1}{2}$ where the radial velocity exceeds its (absolute) value at the wall. At first glance, this behavior appears paradoxical since $u_r$ is expected to diminish monotonically until it vanishes at the centerline. At least, this was the trend observed in the slab rocket motor analogue.[39] The difference here lies
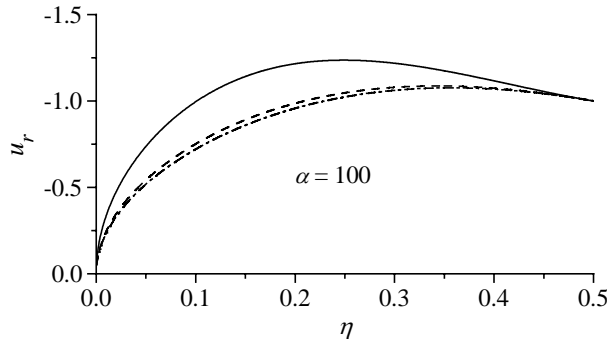
**Fig. 5 Influence of the regression rate on the radial velocity for ——— $R = 100$, - - - - $R = 500$, –·–·– $R = 1000$.**

in the existence of a finite curvature to which one can attribute the near-wall overshoot. The reason is this. Since the cylindrical flow area $A_n(r) = 2\pi rL$ normal to incoming streams is proportional to the radius, the sudden reduction in $A_n$ in the vicinity of the wall (where the axial velocity is insignificant) forces the radial velocity to increase (in absolute value) in order to continue satisfying mass conservation. The second interesting phenomenon is observed when the relative expansion ratio increases. In that event, since expansion delays flow turning, the point of maximum radial velocity moves away from the wall. This is clearly depicted in Fig. 5 for $R = 100$. Past that point of maximum radial velocity, the axial component is no longer insignificant. In that event, the downstream mass transport becomes sufficiently appreciable to offset the effect of a radial compression of $A_n$. For the three cases shown at $\alpha / R = 1, 0.2$, and $0.1$, the radial velocity overshoot relative to the wall is found to be $1.236$, $1.087$, and $1.076$ at $\eta = 0.250, 0.343$, and $0.357$. These points correspond to $r = 0.707, 0.828$, and $0.845$; they indicate that the distance from the wall to the point of maximum $u_r$ is commensurate with the size of $\alpha / R$. We conclude that the closest distance to the wall and smallest overshoot occur when either a) the walls are not moving, or b) the Reynolds number is very high. From the inviscid formulation, one finds that the smallest overshoot is $1.07$ at a radius of $0.861$.

**D.   Radial and Axial Pressure Distribution**

The pressure difference given by Eq. (60) is plotted in Fig. 6 for a) fixed $\alpha$ and a range of $R$, and b) fixed $R$ and a range of $\alpha$. The drop is always positive, indicating, as one would expect, a higher pressure along the centerline. Consistent with the radial velocity distribution, the pressure drop exhibits a maximum on the interval $0 < \eta < \frac{1}{2}$. As shown in Fig. 6a, for $\alpha / R = 1, 0.2$, and $0.1$, extrema of $1.66$, $0.77$, and $0.67$ occur at $r = 0.783, 0.854$, and $0.859$. These locations
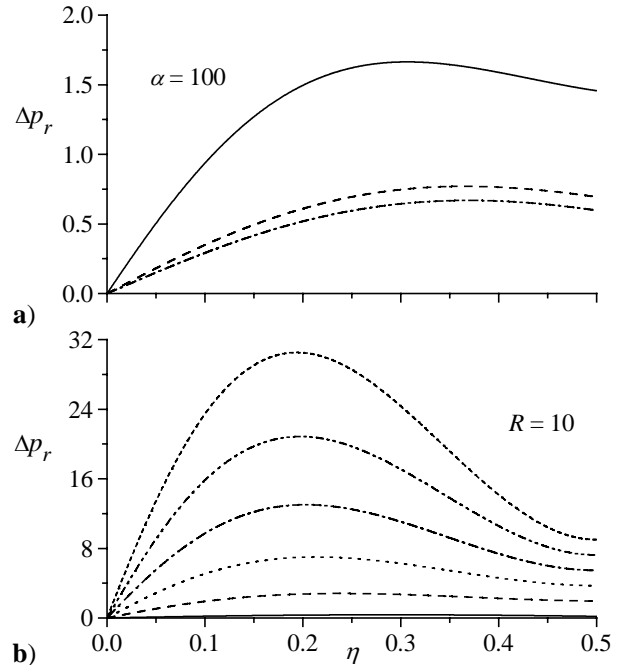


**Fig. 6 a) Influence of the injection Reynolds number on the radial pressure distribution for ——— $R = 100$, - - - - $R = 500$, –·–·– $R = 1000$.   b) Radial pressure distribution at a moderate injection Reynolds number and a range of regression rates: ——— 0, - - - - 20, ······ 40, –··–·· 60, –·–·– 80, ------- 100.**

are 11, 3, and 1.7% closer to the wall than the loci of maximum radial velocities. Both the wall-distance and magnitude of the overshoot seem to decrease with successive decreases in $\alpha / R$. These trends are further confirmed in Fig. 6b where, due to comparable sizes of $\alpha$ and $R$, significant overshoot values in the pressure drop are realized at increasing distances from the wall.

Consistent with Eq. (61), the axial pressure drops in a parabolic fashion along the axis of the tube. Its dependence on $\alpha / R$ follows the same physical arguments presented above.

**E.   Wall Shear Stress**

Lastly, Fig. 7 illustrates the influence of $R$ and $\alpha$ on the shear stress at the expanding wall. For fixed $\alpha$ and a range of $R$, Fig. 7a verifies that the shear stress at the wall decreases with successive increases in the Reynolds number. Thus, as the role of viscosity is diminished, the friction force is weakened as well.

When, in Fig. 7b, the Reynolds number is fixed at $R = 10$, varying the regression rate of comparable size leads to more appreciable stresses at higher expansion rates. The expansion process may therefore be viewed as a mechanism that promotes higher friction at the wall. This stress increases downstream due to the relative growth in the parallel-to-normal velocity ratio.
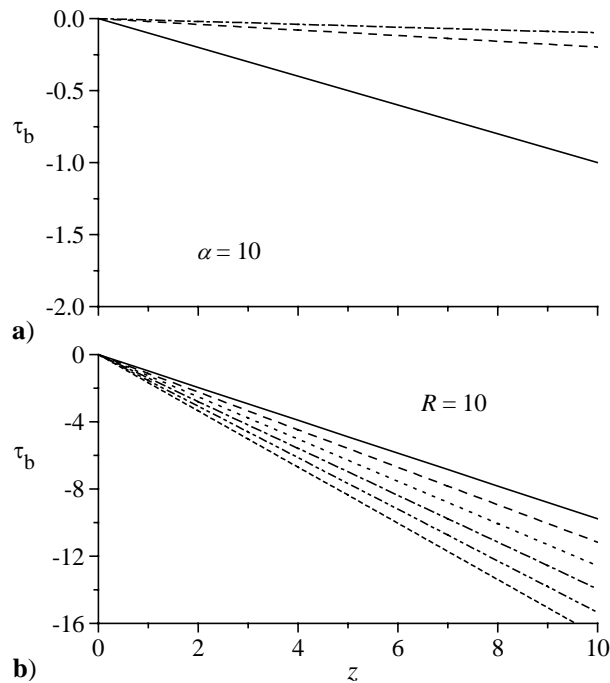
**Fig.7 a) Influence of the injection Reynolds number on the wall shear stress for a moderate regression rate and ──── $R = 100$, - - - - $R = 500$, –·–·– $R = 1000$.
b) Wall shear stress at a moderate injection Reynolds number and a range of regression rates:
──── 0, - - - - 20, ······ 40, –·–·– 60, –··–·· 80, ------- 100.**

## V. Conclusions

In this article, a higher-order mean-flow approximation is presented. In addition to its ability in accounting for wall regression, the solution is consistently viscous and rotational. As such, it is adequate for determining the complete vortico-acoustic solution that has received much scrutiny in the past. It can also be used to investigate, by way of linear stability theory, the hydrodynamic evolution of the mean-flow shear layers. Its applicability over a broader range of physical parameters extends its usage to problems for which the inviscid solution deteriorates. These include high-acceleration interceptor vehicles that utilize high regressive propellants. The details of the mathematical arguments provided here may also be employed in handling other self-similar equations that are exact solutions of the Navier-Stokes equations. In fact, self-similar transformations often lead to fourth-order differential equations whose solutions may be obtained using a similar approach to the one described above. Unlike numerical and experimental studies that have verified the adequacy of Culick's profile,[10] it is reassuring that our formulation, by embracing the inviscid solution at leading order, demonstrates its importance over a range of physical parameters that are characteristic of many solid rocket motors.

## References

[1]Taylor, G. I., "Fluid Flow in Regions Bounded by Porous Surfaces," *Proceedings of the Royal Society, London, Series A,* Vol. 234, No. 1199, 1956, pp. 456-475.
[2]Peng, Y., and Yuan, S. W., "Laminar Pipe Flow with Mass Transfer Cooling," *Journal of Heat Transfer,* Vol. 87, No. 2, 1965, pp. 252-258.
[3]Yuan, S. W., "Cooling by Protective Fluid Films," *Turbulent Flows and Heat Transfer,* Section G, Vol. V, edited by C. C. Lin, Princeton University Press, Princeton, New Jersey, 1959.
[4]Berman, A. S., "Laminar Flow in Channels with Porous Walls," *Journal of Applied Physics,* Vol. 24, No. 9, 1953, pp. 1232-1235.
[5]Berman, A. S., "Effects of Porous Boundaries on the Flow of Fluids in Systems with Various Geometries," *Proceedings of the Second United Nations International Conference on the Peaceful Uses of Atomic Energy, Series P/720,* Vol. 4, 1958, pp. 351-358.
[6]Berman, A. S., "Laminar Flow in an Annulus with Porous Walls," *Journal of Applied Physics,* Vol. 29, No. 1, 1958, pp. 71-75.
[7]Acrivos, A., "The Asymptotic Form of the Laminar Boundary-Layer Mass-Transfer Rate for Large Interfacial Velocities," *Journal of Fluid Mechanics,* Vol. 12, No. 3, 1962, pp. 337-357.
[8]Leadon, B. M., "The Status of Heat Transfer Control by Mass Transfer for Permanent Surface Structures," *Aerodynamically Heated Structures*, edited by P. E. Glaser, Prentice-Hall, Inc., Englewood Cliffs, New Jersey, 1962.
[9]Libby, P. A., "The Homogeneous Boundary Layer at an Axisymmetric Stagnation Point with Large Rates of Injection," *Journal of the Aerospace Sciences,* Vol. 29, No. 1, 1962, pp. 48-60.
[10]Culick, F. E. C., "Rotational Axisymmetric Mean Flow and Damping of Acoustic Waves in a Solid Propellant Rocket," *AIAA Journal,* Vol. 4, No. 8, 1966, pp. 1462-1464.
[11]Hart, R. W., and McClure, F. T., "Combustion Instability: Acoustic Interaction with a Burning Propellant Surface," *The Journal of Chemical Physics,* Vol. 10, No. 6, 1959, pp. 1501-1514.
[12]Terrill, R. M., and Thomas, P. W., "On Laminar Flow through a Uniformly Porous Pipe," *Applied Scientific Research, Series A,* Vol. 21, 1969, pp. 37-67.
[13]Dunlap, R., Willoughby, P. G., and Hermsen, R. W., "Flowfield in the Combustion Chamber of a Solid Propellant Rocket Motor," *AIAA Journal,* Vol. 12, No. 10, 1974, pp. 1440-1445.
[14]Yamada, K., Goto, M., and Ishikawa, N., "Simulative Study of the Erosive Burning of Solid Rocket Motors," *AIAA Journal,* Vol. 14, No. 9, 1976, pp. 1170-1176.
[15]Varapaev, V. N., and Yagodkin, V. I., "Flow Stability in a Channel with Porous Walls," *Fluid Dynamics (Izvestiya Akademii Nauk SSSR, Meckanika Zhidkosti i Gaza),* Vol. 4, No. 5, 1969, pp. 91-95.
[16]Casalis, G., Avalon, G., and Pineau, J.-P., "Spatial Instability of Planar Channel Flow with Fluid Injection through Porous Walls," *The Physics of Fluids,* Vol. 10, No. 10, 1998, pp. 2558-2568.
[17]Beddini, R. A., and Roberts, T. A., "Turbularization of an Acoustic Boundary Layer on a Transpiring Surface," *AIAA Journal,* Vol. 26, No. 8, 1988, pp. 917-923.

[18]Sabnis, J. S., Gibeling, H. J., and McDonald, H., "Navier-Stokes Analysis of Solid Propellant Rocket Motor Internal Flows," *Journal of Propulsion and Power,* Vol. 5, No. 6, 1989, pp. 657-664.

[19]Tissier, P. Y., Godfroy, F., and Jacquemin, P., "Simulation of Three Dimensional Flows inside Solid Propellant Rocket Motors Using a Second Order Finite Volume Method - Application to the Study of Unstable Phenomena," AIAA Paper 92-3275, July 1992.

[20]Roh, T. S., Tseng, I. S., and Yang, V., "Effects of Acoustic Oscillations on Flame Dynamics of Homogeneous Propellants in Rocket Motors," *Journal of Propulsion and Power,* Vol. 11, No. 4, 1995, pp. 640-650.

[21]Apte, S., and Yang, V., "Effects of Acoustic Oscillations on Turbulent Flowfield in a Porous Chamber with Surface Transpiration," AIAA Paper 98-3219, July 1998.

[22]Flandro, G. A., "Solid Propellant Acoustic Admittance Corrections," *Journal of Sound and Vibration,* Vol. 36, No. 3, 1974, pp. 297-312.

[23]Culick, F. E. C., "The Stability of One-Dimensional Motions in a Rocket Motor," *Combustion Science and Technology,* Vol. 7, No. 4, 1973, pp. 165-175.

[24]Flandro, G. A., "Effects of Vorticity Transport on Axial Acoustic Waves in a Solid Propellant Rocket Chamber," *Combustion Instabilities Driven by Thermo-Chemical Acoustic Sources, Nca*, Vol. 4, American Society of Mechanical Engineers, New York, 1989, pp. 53-61.

[25]Majdalani, J., and Van Moorhem, W. K., "The Unsteady Boundary Layer in Solid Rocket Motors," AIAA Paper 95-2731, July 10-12, 1995 1995.

[26]Majdalani, J., and Van Moorhem, W. K., "A Multiple-Scales Solution to the Acoustic Boundary Layer in Solid Rocket Motors," *Journal of Propulsion and Power,* Vol. 13, No. 2, 1997, pp. 186-193.

[27]Kirkköprü, K., Kassoy, D. R., and Zhao, Q., "Unsteady Vorticity Generation and Evolution in a Model of a Solid Rocket Motor," *Journal of Propulsion and Power,* Vol. 12, No. 4, 1996, pp. 646-654.

[28]Majdalani, J., "Improved Flowfield Models in Rocket Motors and the Stokes Layer with Sidewall Injection," Ph.D. Dissertation, University of Utah, 1995.

[29]Majdalani, J., "A Hybrid Multiple Scale Procedure for Boundary Layers Involving Several Dissimilar Scales," *Zeitschrift für angewandte Mathematik und Physik,* Vol. 49, No. 6, 1998, pp. 849-868.

[30]Majdalani, J., and Roh, T. S., "The Oscillatory Channel Flow with Large Wall Injection," *Proceedings of the Royal Society, Series A,* Vol. 456, No. 1999, 2000, pp. 1625-1657.

[31]Flandro, G. A., "Effects of Vorticity on Rocket Combustion Stability," *Journal of Propulsion and Power,* Vol. 11, No. 4, 1995, pp. 607-625.

[32]Flandro, G. A., "On Flow Turning," AIAA Paper 95-2530, July 1995.

[33]Majdalani, J., and Van Moorhem, W. K., "Improved Time-Dependent Flowfield Solution for Solid Rocket Motors," *AIAA Journal,* Vol. 36, No. 2, 1998, pp. 241-248.

[34]Barron, J., Van Moorhem, W. K., and Majdalani, J., "A Novel Investigation of the Oscillatory Field over a Transpiring Surface," *Journal of Sound and Vibration,* Vol. 235, No. 2, 2000, pp. 281-297.

[35]Brown, R. S., Blackner, A. M., Willoughby, P. G., and Dunlap, R., "Coupling between Velocity Oscillations and Solid Propellant Combustion," Final Technical Rept. F49620-81-C-0027, Bolling Air Force Base, Washington DC, August 1986.

[36]Dunlap, R., Blackner, A. M., Waugh, R. C., Brown, R. S., and Willoughby, P. G., "Internal Flow Field Studies in a Simulated Cylindrical Port Rocket Chamber," *Journal of Propulsion and Power,* Vol. 6, No. 6, 1990, pp. 690-704.

[37]Majdalani, J., "The Boundary Layer Structure in Cylindrical Rocket Motors," *AIAA Journal,* Vol. 37, No. 4, 1999, pp. 505-508.

[38]Majdalani, J., "The Oscillatory Channel Flow with Arbitrary Wall Injection," *Zeitschrift für angewandte Mathematik und Physik,* Vol. 52, No. 1, 2001, pp. 33-61.

[39]Majdalani, J., and Van Moorhem, W. K., "Laminar Cold-Flow Model for the Internal Gas Dynamics of a Slab Rocket Motor," *Journal of Aerospace Science and Technology,* Vol. 5, No. 3, 2001, pp. 193-207.

[40]Yuan, S. W., "Further Investigation of Laminar Flow in Channels with Porous Walls," *Journal of Applied Physics,* Vol. 27, No. 3, 1956, pp. 267-269.

[41]Zhou, C., and Majdalani, J., "Improved Mean-Flow Solution for Slab Rocket Motors with Regressing Walls," AIAA Paper 2000-3191, July 2000.

[42]Goto, M., and Uchida, S., "Unsteady Flows in a Semi-Infinite Expanding Pipe with Injection through Wall," *Transactions of the Japan Society for Aeronautical and Space Sciences,* Vol. 33, No. 9, 1990, pp. 14-27.

[43]Yuan, S. W., and Finkelstein, A. B., "Laminar Pipe Flow with Injection and Suction through a Porous Wall," *Transactions of the American Society of Mechanical Engineers: Journal of Applied Mechanics, Series E,* Vol. 78, 1956, pp. 719-724.

[44]Ma, Y., Van Moorhem, W. K., and Shorthill, R. W., "Innovative Method of Investigating the Role of Turbulence in the Velocity Coupling Phenomenon," *Journal of Vibration and Acoustics-Transactions of the ASME,* Vol. 112, No. 4, 1990, pp. 550-555.

[45]Ma, Y., Van Moorhem, W. K., and Shorthill, R. W., "Experimental Investigation of Velocity Coupling in Combustion Instability," *Journal of Propulsion and Power,* Vol. 7, No. 5, 1991, pp. 692-699.

[46]Sutton, G. P., *Rocket Propulsion Elements*, 6th ed., John Wiley & Sons, Inc., New York, 1992.

[47]Reid, R. C., Prausnitz, J. M., and Poling, B. E., *The Properties of Gases and Liquids*, 4th ed., McGraw Hill, New York, 1987, p. 388–490.

[48]Beckstead, M., "Overview of Combustion Mechanisms and Flame Structures for Advanced Solid Propellants," *Solid Propellant Chemistry, Combustion, and Motor Interior Ballistics*, Vol. 185, edited by V. Yang, T. B. Brill, and W.-Z. Ren, Progress in Astronautics and Aeronautics, Washington, DC, 2000, pp. 267-285.

[49]Uchida, S., and Aoki, H., "Unsteady Flows in a Semi-Infinite Contracting or Expanding Pipe," *Journal of Fluid Mechanics,* Vol. 82, No. 2, 1977, pp. 371-387.

[50]Terrill, R. M., "On Some Exponentially Small Terms Arising in Flow through a Porous Pipe," *Quarterly Journal of Mechanics and Applied Mathematics,* Vol. 26, No. 3, 1973, pp. 347-354.